the plant journal

SEB SOCIETY FOR EXPERIMENTAL BIOLOGY

The Plant Journal (2025) **124,** e70608 doi: 10.1111/tpj.70608

Functional analysis of a GWAS pleiotropic hotspot suggests an auxin biosynthesis gene (*AhPDS1*), regulating pod development in peanut (*Arachis hypogaea* L.)

Qing Lu[1,*,†], Muhammad J. Umer[1,†], Hao Liu[1,*], Haifen Li[1], Runfeng Wang[1], Lu Huang[1], Qianxia Yu[1], Rajeev K. Varshney[2], Manish K. Pandey[3], Yanbin Hong[1,*] and Xiaoping Chen[1,*]

[1]*Crops Research Institute, Guangdong Academy of Agricultural Sciences, Guangdong Provincial Key Laboratory of Crop Genetic Improvement, South China Peanut Sub-Centre of National Centre of Oilseed Crops Improvement, Guangzhou, China,*

[2]*WA State Agricultural Biotechnology Centre, Centre for Crop and Food Innovation, Food Futures Institute, Murdoch University, Murdoch, Western Australia, Australia, and*

[3]*International Crops Research Institute for the Semi-Arid Tropics (ICRISAT), Hyderabad, India*

Received 27 December 2024; revised 10 November 2025; accepted 12 November 2025.

*For correspondence (e-mail luqing@gdaas.cn and liuhao@gdaas.cn and hongyanbin@gdaas.cn and chenxiaoping@gdaas.cn).

†These authors contributed equally to this work.

SUMMARY

Peanut productivity and quality improvement rely on understanding the genetic factors influencing pod and seed size. This study aims to identify genetic factors and regulatory mechanisms influencing pod and seed size in peanuts. Herein, a genome-wide association study (GWAS) was conducted using 390 accessions from 15 peanut growing regions to analyze pod and seed traits across multiple planting seasons. A significant phenotypic variation was observed, with broad-sense heritability ranging from 53.6 to 85.4%. Strong correlations between pod and seed traits further suggest potential for co-selection in breeding efforts. A pleiotropic hotspot on chromosome B06 was strongly associated with six pod and seed traits. A peanut pod size regulator *AhPDS1* (*PODSIZE-1, Ahy_B06g085516*) homolog of *Arabidopsis thaliana YUCCA4* (*AtYUC4, AT5G11320*), involved in auxin biosynthesis, was selected as a candidate regulating pod and seed size. Quantitative reverse transcriptase-polymerase chain reaction (qRT-PCR) confirmed higher *AhPDS1* expression in large pod as compared with the small pod genotypes. Subcellular localization showed *AhPDS1* to be predominantly cytoplasmic, and GUS reporter assays indicated widespread expression in roots, stems, leaves, flowers, and pods, suggesting a broad functional role. Further overexpression of *AhPDS1* in Arabidopsis and rice enhanced pod, seed, and grain sizes via the indole-3-pyruvic acid pathway in transgene lines. These findings highlight *AhPDS1* as a potential target for peanut molecular breeding, offering opportunities to enhance pod size via auxin biosynthesis and support sustainable crop improvement.

Keywords: peanut, GWAS, *AhPDS1*, auxin biosynthesis, molecular breeding.

INTRODUCTION

The cultivated peanut (*Arachis hypogaea* L.), also called groundnut, is an important oilseed crop. It is widely cultivated in more than 143 countries, especially in America, India, and China, with ~50 million tons produced worldwide on an area of 29 million hectares. Stagnant peanut production cannot meet the rising demand; thus, it is urgent to enhance peanut production through molecular breeding to fulfill the desired needs. Cultivated peanut is an allotetraploid (AABB, $2n = 4\times = 40$), thought to be derived from hybridization between diploids *Arachis duranensis* (A genome) and *Arachis ipaensis* (B genome) (Robledo et al., 2009; Seijo et al., 2007; Smartt et al., 1978) which have already been sequenced (Bertioli et al., 2016; Chen, Li, et al., 2016; Lu, Li, et al., 2018). Yield is a major focus of breeding, which is directly influenced by pod and seed size-related traits (López-Bellido et al., 2005). Therefore, it is necessary to understand the genetic basis of pod- and seed-related traits for genetic improvement using marker-assisted selection.

Linkage mapping based on biparental crossing populations is a routine strategy for quantitative trait loci (QTLs) identification, including peanut pod and seed size (Chavarro et al., 2020; Chen, Jiao, et al., 2016; Huang

et al., 2015; Meijie et al., 2019; Shirasawa, Endo, et al., 2012; Shirasawa, Koilkonda, et al., 2012). In addition, QTL identification based on multiparental mapping populations, such as a nested-association mapping (NAM) or multiparent advanced generation inter-cross (MAGIC), shows great potential for genetic mapping in maize (Yan et al., 2011), rice (Fragoso et al., 2017), tomato (Campanelli et al., 2019), soybean (Xavier et al., 2018), and cotton (Wang, Ma, et al., 2022) benefiting from their additional recombination breakpoints and allelic diversity. In peanut, the recombinant inbred line (RIL) population was derived from a cross between Tifrunner (a dormant Runner-type) and GT-C20 (a non-dormant Spanish-type). Genotyping with the 58K 'Axiom_Arachis' single-nucleotide polymorphism (SNP) array enabled the identification of two major QTLs for seed dormancy on chromosomes A04 and A05, which explain 43.16 and 51.61% of the phenotypic variation (PVE), respectively (Wang, Wang, et al., 2022). Moreover, two NAM populations, NAM_Tifrunner and NAM_Florida-07, were established to dissect the genetic control of pod weight (PW) and seed weight (SW) in peanut. This multiparental approach is highly effective for investigating quantitative traits and enables the rapid discovery of candidate genes and markers (Gangurde et al., 2020). However, the construction of these bi or multiparental mapping populations was laborious and time consuming.

Genome-wide association study (GWAS) based on extensive historic recombination in a large diverse natural population has proven to be an excellent approach for the identification of important causal loci, genes, etc. Recently, QTLs for important agronomic traits have been identified by GWAS in several crops (Chen et al., 2025; Jha et al., 2025; Sharma & Chahota, 2025; Umer et al., 2024; Yang, Gu, et al., 2025). In recent years, two peanut wild diploid progenitors, *A. ipaensis* and *A. duranensis* (Bertioli et al., 2016; Chen et al., 2019; Chen, Li, et al., 2016; Leal-Bertioli et al., 2017; Lu et al., 2019), an allotetraploid wild peanut *Arachis monticola* (Yin et al., 2018) and allotetraploid cultivated peanut *A. hypogaea* (Bertioli et al., 2019; Chen et al., 2019; Zhuang et al., 2019) have been successfully assembled by different international peanut research organizations. These *Arachis* reference genomes have provided abundant genomic resources to develop high-resolution genetic markers (Lu et al., 2019; Pandey et al., 2017; Zhao et al., 2017) and for sequence-based trait mapping and candidate gene mining (de Blas et al., 2021; Huang et al., 2023; Raza et al., 2024; Sun et al., 2022; Zhou et al., 2021). In addition, GWAS for pod and seed-related traits have also already been carried out and yielded several candidate genes in peanut (Chen et al., 2025; Patel et al., 2022; Yang, Yue, et al., 2025; Zhang et al., 2023). However, GWAS based on resequencing of large-scale germplasm resources to mine pod and seed size-associated QTLs (or genes) is not adequate in peanut.

In this research, a GWAS utilizing resequencing genotypes was conducted to examine traits related to pod and seed size in 390 globally collected peanut accessions. The primary objectives of the study were: to identify novel genetic associations linked to traits related to pod and seed size, to pinpoint and confirm potential candidate genes, and to offer a set of target loci that can be used for molecular breeding of peanut cultivars. The findings are expected to elucidate the biological mechanisms governing pod and seed size, thereby providing valuable markers for future peanut breeding initiatives.

RESULTS

Plant material and PVE

A collection of 390 accessions, predominantly sourced from 15 different peanut-growing countries or regions was utilized to form a GWAS mapping panel (Lu, Huang, Liu, Garg, Gangurde, Li, Chitikineni, Guo, Pandey, Li, Wang, et al., 2024) (Figure 1a). This panel was used to analyze pod and seed size related traits (Figure 1b). Specifically, we examined pod length (PL), pod width (PW), pod thickness (PT), hundred-pod weight (HPW), seed length (SL), seed width (SW), seed thickness (ST), and hundred-seed weight (HSW) across four planting seasons. Analysis revealed a broad range of PVEs for each of these traits, with continuous variation and almost normal distributions observed across the different environments (Table 1; Figure 1c). This indicates a diverse genetic background among the accessions studied, providing a robust basis for GWAS. The broad-sense heritability (H_B^2%) for the traits related to pod and seed size was found to range between 53.3 and 85.4% (Table 1). This high level of heritability suggests that a significant portion of the PVE in these traits can be attributed to genetic factors, making them reliable traits for genetic studies and selection in breeding programs.

Furthermore, Pearson correlation analysis demonstrated highly significant phenotypic correlations between various combinations of pod and seed size related traits across the four testing environments. Notably, there was a strong correlation between PT and PW ($r = 0.912$, $P < 0.001$), as well as between HSW and HPW ($r = 0.857$, $P < 0.001$) (Figure 1c). These strong correlations indicate that certain traits are closely linked and could be co-selected in breeding programs aimed at improving peanut yield and quality.

GWAS for seed and pod size traits

Genome-wide association analysis yielded a total of 883 significant SNP-trait associations across eight pod and seed size related traits in four environments (Figure S1). These associations were not randomly distributed, but instead formed distinct chromosomes and regions of

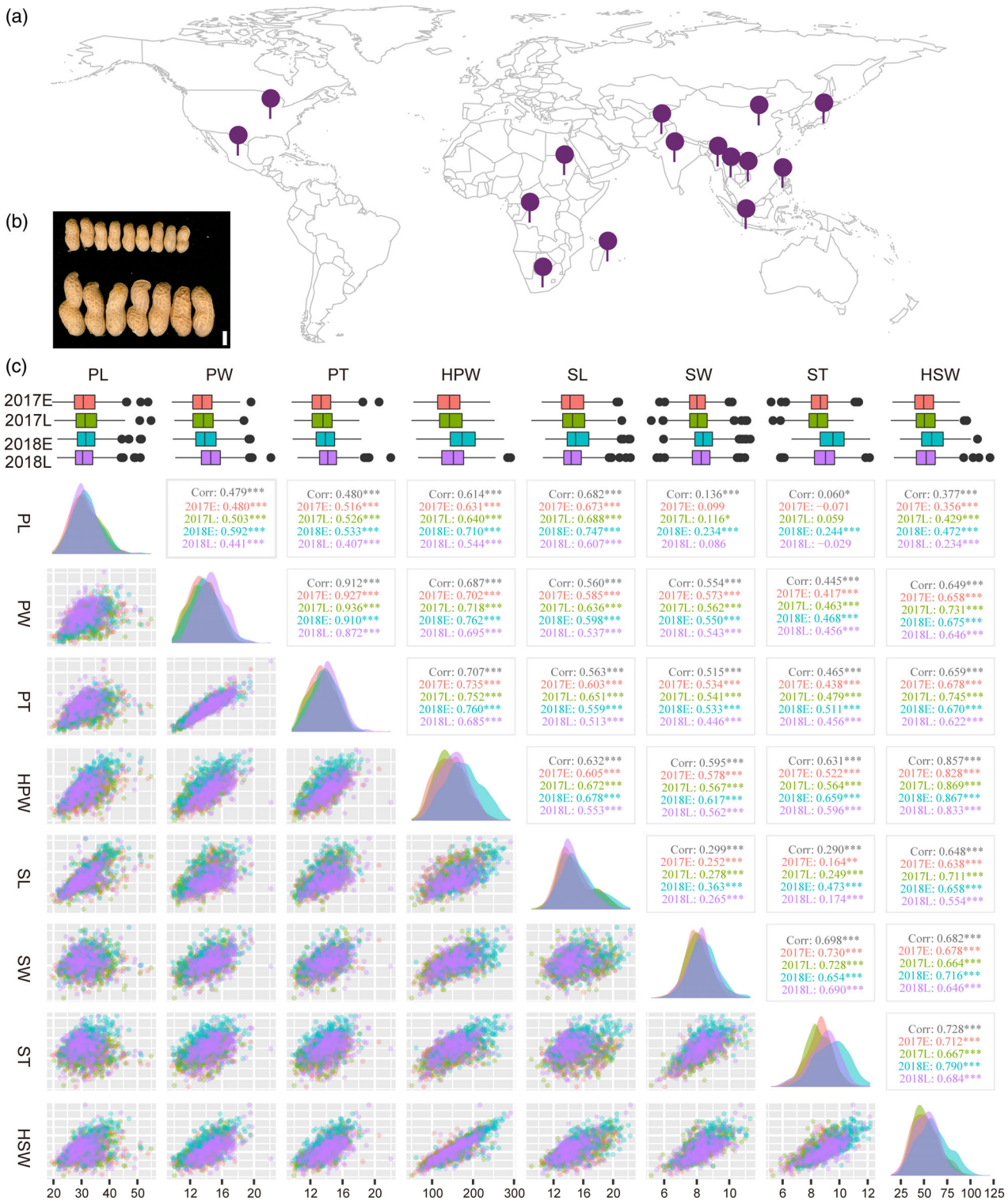

Figure 1. Material distribution and pod and seed size diversity.
(a) The geographical origins of peanut accessions used in this study. The accessions were predominantly sourced from 15 different peanut growing countries or regions, highlighting the global diversity of the peanut varieties analyzed. The map provides an overview of the collection sites, showcasing the wide distribution of the accessions.
(b) Peanut accessions with phenotypic variations among pod sizes.
(c) Pearson correlation analysis was conducted to evaluate the phenotypic correlations between various combinations of pod and seed related traits across four different testing environments. Whereas, *, **, *** indicates $P < 0.05$, $P < 0.01$, $P < 0.001$ respectively.

Table 1 Phenotypic variations of pod and seed size traits in four environments

Trait	Environment[a]	Mean	SE[b]	Minimum	Maximum	H_B^2 (%)[c]
Pod length (mm)	2017E	31.28	0.27	19.46	53.78	85.4
	2017L	31.85	0.26	20.26	54.86	
	2018E	32.02	0.26	21.41	51.47	
	2018L	31.08	0.24	21.29	51.05	
Pod width (mm)	2017E	13.55	0.08	9.71	19.63	75.2
	2017L	13.64	0.09	10.03	18.75	
	2018E	13.98	0.10	9.84	19.54	
	2018L	14.66	0.09	10.13	22.12	
Pod thickness (mm)	2017E	13.45	0.08	9.68	20.53	78.7
	2017L	13.48	0.08	9.98	18.08	
	2018E	13.81	0.08	9.81	18.34	
	2018L	14.21	0.09	10.42	21.98	
Hundred-pod weight (g)	2017E	142.64	1.92	54.50	242.00	70.3
	2017L	145.82	1.92	49.92	252.80	
	2018E	175.38	2.22	61.20	275.45	
	2018L	151.88	1.92	66.00	291.67	
Seed length (mm)	2017E	14.74	0.11	10.41	20.75	82.6
	2017L	14.86	0.11	9.03	21.16	
	2018E	15.42	0.12	10.90	22.28	
	2018L	14.62	0.09	10.58	22.32	
Seed width (mm)	2017E	8.03	0.04	5.71	10.18	58.9
	2017L	8.13	0.04	5.20	11.08	
	2018E	8.44	0.05	5.96	11.29	
	2018L	8.28	0.04	5.55	10.95	
Seed thickness (mm)	2017E	8.59	0.05	5.18	11.36	53.3
	2017L	8.48	0.05	5.32	11.00	
	2018E	9.50	0.06	6.62	12.17	
	2018L	8.90	0.06	5.84	12.13	
Hundred-seed weight (g)	2017E	51.17	0.74	15.96	88.68	74.6
	2017L	51.97	0.71	14.40	96.00	
	2018E	59.70	0.86	24.15	107.62	
	2018L	52.57	0.73	17.58	121.05	

[a]E, early season (from April and July of each year in Guangzhou, China); L, late season (from August and November of each year in Guangzhou, China).
[b]SE, standard error.
[c]H_B^2 (%), broad-sense heritability.

association (Figure S2). Several hotspots were identified on chromosomes A02, A03, A05, A06, A07, A09, and B06 (Table S1; Figure S3). For example, a prominent region on chromosome B06 (B06.1; 142.8–149.2 Mb) encompassed associations with six traits (PW, PT, HPW, SL, SW, and HSW), consistent with previous QTLs reported for PW and SW (Chavarro et al., 2020). Likewise, clusters of associations on A05 and A09 overlapped with loci identified in NAM and RIL populations (Gangurde et al., 2020, 2023), reinforcing their reliability. Importantly, several loci were repeatedly detected across environments, underscoring their stability. These include a region on chromosome A09 (8.04–8.61 Mb) for PL, a region on chromosome B06 (143.4–145.3 Mb) for PW and PT, and a locus on chromosome A05 (9.82 Mb) for SL (Table S2; Figure S4). Additionally, a PL associated locus on Scaffold 6 (211 kb) was consistently detected in two environments (2017E and 2018E). Such stable regions provide strong candidates for fine mapping, candidate gene identification, and molecular breeding applications.

Genetic analysis of a pleiotropic hotspot on chromosome B06 associated with pod and seed traits

A pleiotropic hotspot (B06.1) on chromosome B06 was identified that is significantly associated with six pod and seed related traits, including PW, PT, HPW, SL, SW, and HSW, across multiple environments (Figure 2a; Figure S3). The candidate hotspot core region covering most of the significant associations, spans approximately 1.5 Mb, from 143.6 to 145.1 Mb (Figure 2b). Genome-wide selective sweep analysis indicated that this region has high artificial selection, suggesting strong selection pressure on this hotspot for pod and seed traits (Lu, Huang, Liu, Garg, Gangurde, Li, Chitikineni, Guo, Pandey, Li, Wang, et al., 2024) (Figure 2c). Linkage disequilibrium (LD) block analysis of the hotspot core region identified three

blocks, with the first block, ranging from 143.56 to 143.75 Mb (~186.21 kb), containing multiple pleiotropic lead or second lead SNPs associated with pod and seed traits across different environments (Figure 2d). This block includes 10 predicted genes (Figure 2f; Table S3), with one notable gene, *Ahy_B06g085516*, annotated as an indole-3-pyruvate monooxygenase named *PODSIZE-1* (*AhPDS1*). *AhPDS1* showed significantly higher expression in large pod (LP) genotypes when compared with small pod (SP) genotypes (Figure S5). Moreover, *AhPDS1* is a homolog of *A. thaliana YUCCA4* (*AtYUC4*, *AT5G11320*), annotated as an indole-3-pyruvate monooxygenase involved in auxin biosynthesis (Zhao, 2012) (Figure S6A, B). Resequencing of 390 accessions revealed a non-synonymous SNP (C/A) in the fourth exon of *AhPDS1*, resulting in two main genotypes (CC and AA) and leading to an amino acid change from asparagine to lysine (Figure 2g). Accessions with the CC genotype tended to have larger pod and seed sizes than those with the AA genotype, with significant differences observed for several measured traits (Figure 2h). To further investigate the potential functional impact of this non-synonymous substitution on *AhPDS1* protein structure and activity, we conducted a comprehensive *in silico* analysis integrating sequence conservation, structural modeling, and stability prediction approaches. Our analysis focused primarily on the N402K substitution, which consistently emerged as potentially deleterious. Using the Missense3D tool, we identified this mutation as 'Damaging', primarily due to an alteration in a protein cavity an area typically critical for substrate interaction or catalytic activity. This structural perturbation was corroborated by stability predictions from I-Mutant 2.0 and MutPro, both of which indicated reduced protein stability, suggesting a possible compromise in the enzyme's structural integrity. To further explore the biochemical implications, we employed the HOPE tool, which provided additional insights despite the absence of an experimentally resolved YUC4 3D structure. The HOPE analysis revealed that the N402K substitution introduces a positively charged lysine residue in place of a neutral asparagine, potentially causing electrostatic repulsion or steric clashes with nearby residues or ligands. Moreover, the mutation occurs within a turn region typically favored by asparagine, indicating possible local destabilization due to the distinct structural preferences of lysine (Figure S6C). Although the residue itself is not highly conserved and the lysine substitution appears in certain homologs, the overall convergence of our structural and stability analyses strongly supports a deleterious functional impact. Overall, the collective evidence from multiple independent computational approaches including cavity alteration, reduced protein stability, and a non-conservative charge and size substitution supports the conclusion that the N402K mutation likely impairs YUC4 enzyme function. These findings provide a mechanistic explanation for the PVE observed between the *AhPDS1* haplotypes.

Expression dynamics, quantification of indole-3-acetic acid (IAA), and subcellular localization of *AhPDS1*

Sequencing analysis detected no variations in the promoter region but identified four SNP variations in the coding sequence (CDS) region between the LP and the SP varieties, resulting in two amino acid changes indicating a potential role of *AhPDS1* in pod size regulation across developmental phases (Figure 3a,b; Figure S7). The results of IAA content measurement at different pod developmental stages of the contrasting peanut genotypes LP and SP revealed a dynamic pattern of IAA accumulation, with levels being relatively higher during the early pod developmental stages (S0–S3), followed by a noticeable decline at the later stages (S4–S5). Importantly, across different pod developmental stages, the LP genotype consistently exhibited significantly higher IAA levels compared with the SP genotype (Figure 3b). To examine the effects of auxin and its transport inhibitors on pod development, exogenous treatments of IAA, N-1-naphthylphthalamic acid (NPA), and 2,3,5-triiodobenzoic acid (TIBA) were applied to contrasting peanut genotypes, LP and SP (Figure S8A). At a concentration of 1 μM, exogenous IAA significantly increased PL in both genotypes, with a stronger response observed in LP compared with SP. NPA treatment also caused a moderate increase in pod size relative to the control, although the effect was less pronounced than IAA. In contrast, TIBA treatment markedly reduced PL, PW, and PT, indicating its strong inhibitory effect on pod growth (Figure S8B–D). At the higher concentration of 10 μM, TIBA treatment was toxic, leading to plant death within 5 days, likely due to excessive inhibition of auxin transport. In contrast, exogenous IAA further enhanced PL in both genotypes, whereas the effects on PW and PT were moderate and not statistically significant in SP (Figure S8E–G). NPA treatment at this concentration suppressed pod elongation relative to IAA, but plants remained viable, suggesting that partial inhibition of auxin transport restricts pod expansion without lethality. Overall, these results demonstrate that exogenous IAA promotes pod elongation, whereas auxin transport inhibitors (TIBA and NPA) constrain pod growth. The consistent reduction in pod size traits under inhibitor treatments supports the conclusion that proper auxin homeostasis and transport are essential for peanut pod development. The qRT-PCR results across different tissues (roots, stems, leaves, flowers, and pods) of LP and SP revealed distinct expression patterns of *AhPDS1*. In LP genotypes, *AhPDS1* was predominantly expressed in leaves and pods, whereas in SP genotypes its expression was comparatively higher in flowers (Figure 3c). Overall,

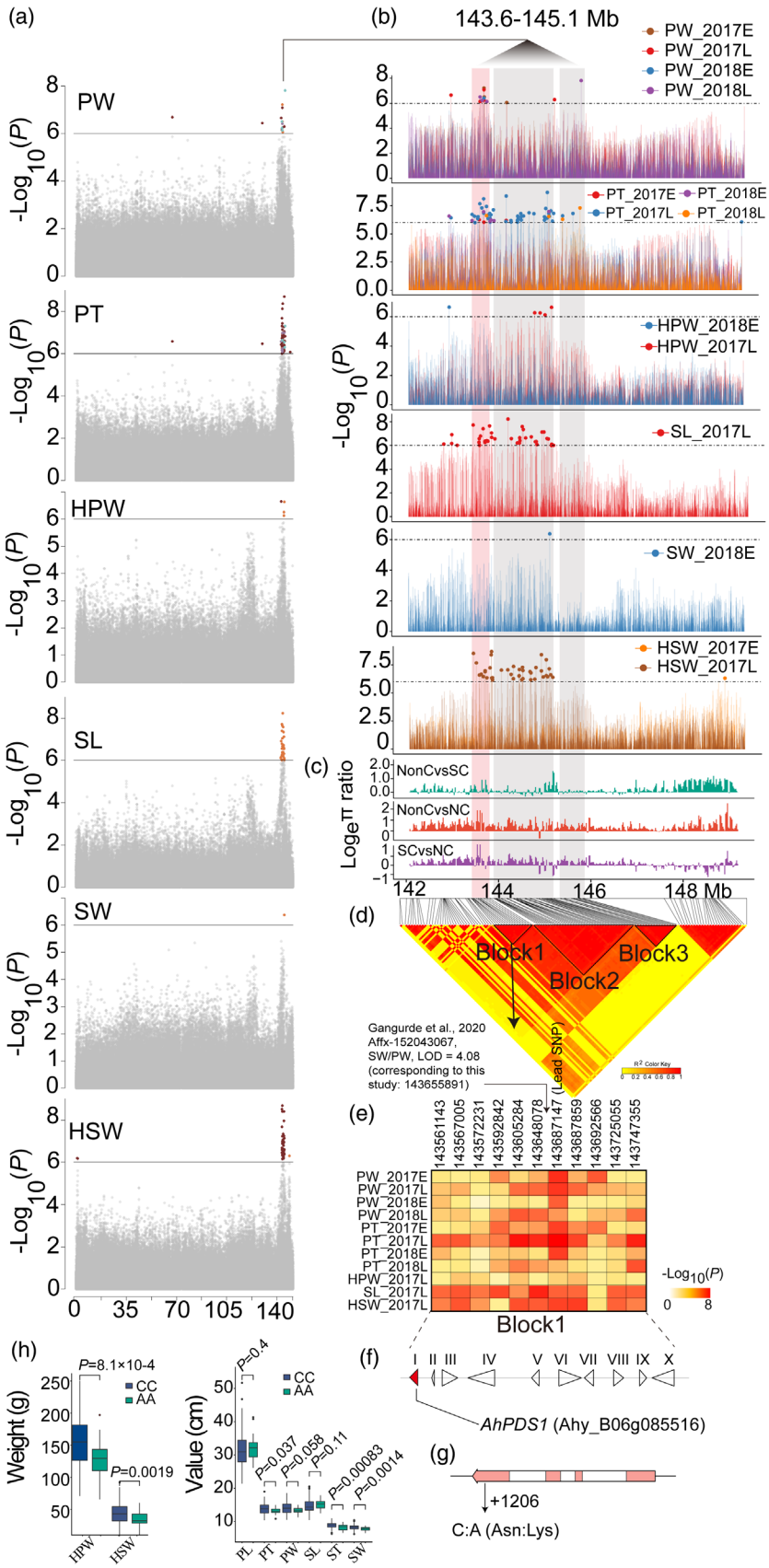

Figure 2. Genome-wide association study for pod and seed size related traits and candidate gene identification.
(a, b) Manhattan plots displaying single-nucleotide polymorphisms (SNPs) associated with pod and seed size related traits on chromosome B06 in peanut. The horizontal dashed line represents the genome-wide significance threshold ($P = 1 \times 10^{-6}$), determined by Bonferroni correction to reduce false positives.
(c) Selective sweep analysis on chromosome B06, indicating regions of reduced genetic diversity, which might have been subject to strong positive selection during domestication whereas, NonC means Non-China, SC means South China and NC means North China as described in our previous publication (Lu, Huang, Liu, Garg, Gangurde, Li, Chitikineni, Guo, Pandey, Li, Liu, et al., 2024).
(d) Linkage disequilibrium (LD) heatmap for the top SNPs identified in this study, which are associated with pod length.
(e) The heatmap shows the $-\log_{10}$ (*P*-value) of each SNP in LD Block 1, with the most significant SNP. This SNP is associated with the candidate gene *AhPDS1*.
(f) Putative gene models within the candidate LD block region (143.56–143.75 Mb; ~186 kb). The region contains 10 predicted genes, with the candidate gene (*AhPDS1*) shown by a red triangle.
(g) Gene structure of *AhPDS1* highlighting a non-synonymous SNP located in the fourth exon (C/A substitution). This SNP leads to an amino acid change.
(h) Box plot comparing pod and seed sizes in different accessions. Accessions with the CC genotype showed significantly larger pod and seed sizes compared with accessions with the AA genotype, suggesting a strong association between this genotype and size traits. In the boxplot (h), the centerline represents the median; box lower and upper edges represent the 25 and 75% quartiles, respectively; whiskers represent 1.5× IQR; and dots represent outliers. *P*-values were calculated by two-tailed Student's *t*-test.

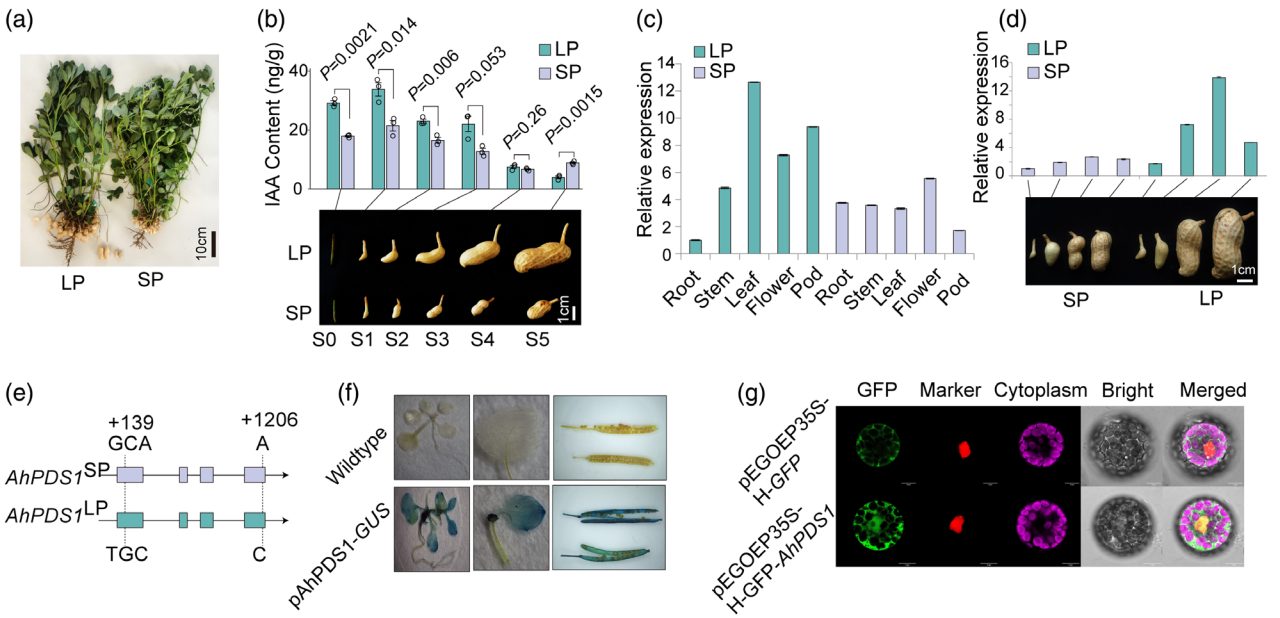

Figure 3. Gene expression and subcellular localization of *AhPDS1*.
(a) Phenotypic comparison of peanut varieties with large (LP) and small pod (SP) sizes. The image shows the physical differences between peanuts with larger and smaller pods, highlighting the variation in pod size. Scale bar = 10 cm.
(b) Measurement of indole-3-acetic acid content (ng/g) in LP and SP peanuts at different pod developmental stages (0–5).
(c) Expression of *AhPDS1* in different peanut tissues (root, stem, leaf, flower and pod) of SP and LP peanuts.
(d) Expression dynamics of *AhPDS1* in peanut varieties with differing pod sizes (small and large). The changes in the expression levels of *AhPDS1* in relation to pod size, indicate its potential role in pod development. Scale bar = 1 cm.
(e) Single-nucleotide polymorphism variations in the coding sequence region between the LP and the SP varieties.
(f) The histochemical analysis of *AhPDS1* promoter activity in various Arabidopsis tissues. The transgenic Arabidopsis plants expressing pAhPDS1-*GUS* displayed GUS activity in roots, leaves, and pods, as indicated by the blue staining.
(g) Subcellular localization of *AhPDS1* protein in peanut leaf cell protoplasts. The construct pEGOEP35S-H-*GFP-AhPDS1* was transiently expressed in the protoplasts, and the green fluorescent protein (GFP) signal (green) was detected throughout the cytoplasm. The bright field image provides a visual reference for the protoplast structure, and the merged image shows the overlap of the GFP signal with the bright field image. A control construct (pEGOEP35S-H-*GFP*) expressing only the GFP protein was used to demonstrate the localization pattern specific to *AhPDS1*. The red signal corresponds to a nuclear marker, highlighting the absence of *AhPDS1* in the nucleus. Scale bar = 10 μm. Data in (b–d) are given as mean ± SE with three replications. *P*-values were calculated by two-tailed Student's *t*-test.

qRT-PCR further demonstrated a significant upregulation of *AhPDS1* in LP varieties carrying the TGC/CC genotype, relative to SP varieties with the GCA/AA genotype. The increased expression was particularly notable during the critical pod expansion stages (Figure 3d). This differential expression pattern suggests that *AhPDS1* is actively involved in regulating pod growth, likely contributing to the observed differences in pod size between the accessions. The elevated expression of *AhPDS1* in LP genotypes points to its potential role as a key genetic factor in pod development, influencing both the rate and extent of pod enlargement.

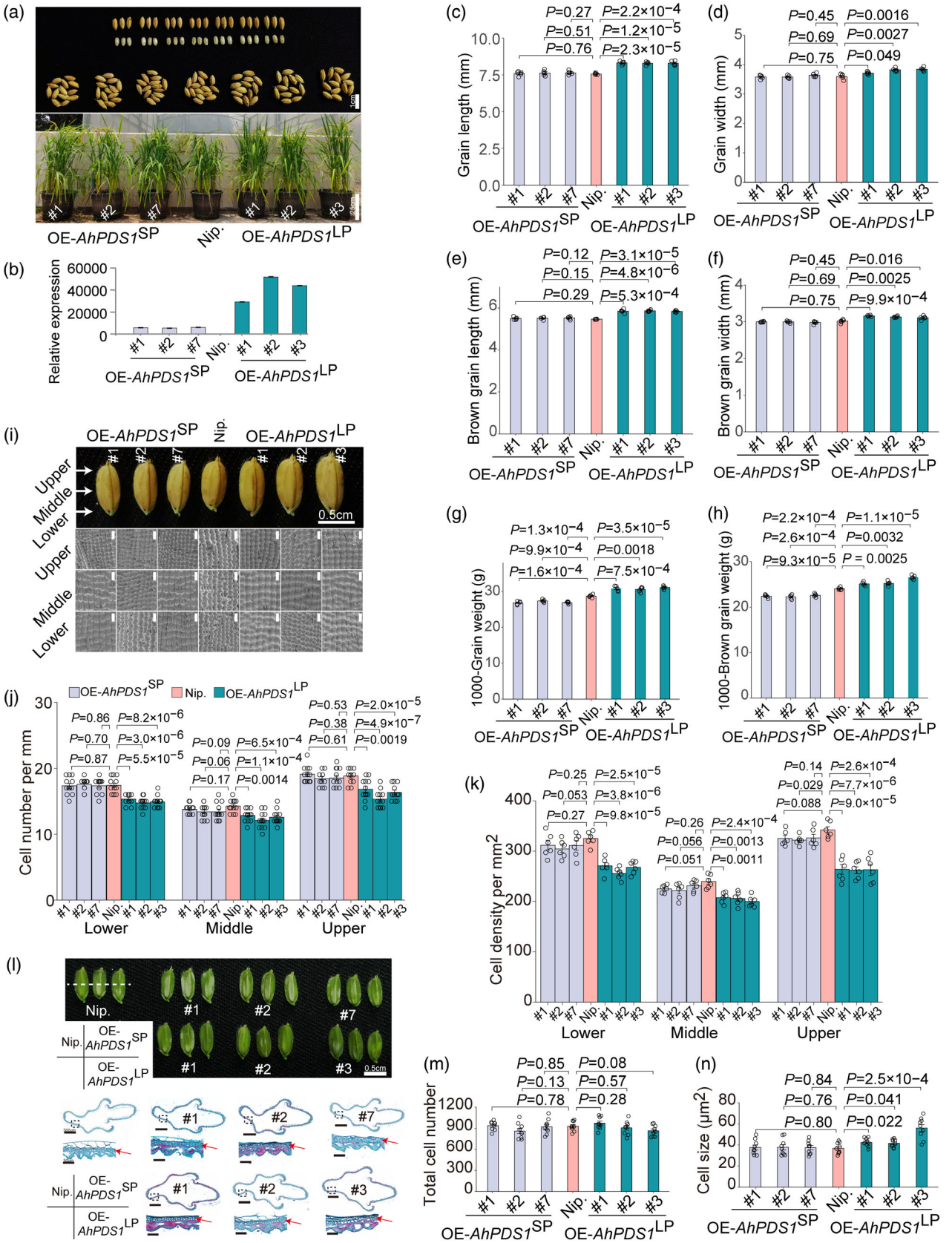

Figure 4. Comparative analysis of grain morphology in rice overexpressing the *AhPDS1* gene.
(a) Plant, grain, and brown grain morphology of wild-type Nipponbare (Nip.) and two *AhPDS1* haplotypes overexpressed lines in the spring season at Guangzhou. Upper scale bars = 1 cm, and lower scale bars = 25 cm, respectively.
(b) Expression analysis of *AhPDS1* in the generated transgenic lines.
(c–h) Bar graphs showing the comparison of grain and brown grain morphological traits and weights, including grain length (mm) (c), grain width (mm) (d), brown grain length (mm) (e), brown grain width (mm) (f), 1000 grain weight (g) (g), and 1000 brown grain weight (h) between wild-type Nip. and transgenic rice lines (OE-*AhPDS1*^{LP} and OE- *AhPDS1*^{SP}).
(i) Scanning electron and light microscope photographs of the outer surfaces of mature grains. Scale bar, 0.5 cm for whole seeds and 100 μm for lemma.
(j) Cell number per millimeter and (k) cell density per square millimeter in the upper, middle, and lower positions of hulls along the longitudinal axis.
(l) Spikelet on the heading day with a scale bar, 0.5 cm and cross-sections of the central part of the spikelet hull (white dashed lines). A magnified view of each boxed cross-section is shown at the bottom. Arrows indicate outer parenchymal cell layers. Scale bars, 500 μm (upper) and 50 μm (lower).
(m) Total cell number and (n) cell size in the outer parenchymal cell layers of spikelet. Data in (b–h, j, k, m, and n) are given as mean ± SE with three replications; *n* = 3, 5, 12, 6, and 9 samples for (c–h, j, k m, and n), respectively. *P*-values were calculated by two-tailed Student's *t*-test.

The GUS staining revealed that *AhPDS1* is expressed in multiple tissues, including roots, leaves, and pods (Figure 3f). The expression in these tissues indicates a potentially broad role for *AhPDS1* in plant growth and development, possibly influencing a range of physiological processes across different organ systems. Together, these findings indicate that *AhPDS1* plays a critical and multifaceted role in peanut pod development by regulating growth at both the tissue and cellular levels, making it a key gene for further investigation in the context of improving peanut growth and yield. To investigate the subcellular localization of *AhPDS1*, a green fluorescent protein (GFP)-tagged *AhPDS1* construct was transiently expressed. The fluorescent signals were observed extensively throughout the cytoplasm, indicating that *AhPDS1* is predominantly localized within the cytoplasm of peanut cells. This localization was further confirmed by the absence of GFP signals in the nucleus, as evidenced by the lack of co-localization with the nuclear marker (shown in red) (Figure 3g). These observations suggest that *AhPDS1* does not localize to specific organelles but rather remains cytoplasmic.

Overexpression of *AhPDS1* enhances grain size in rice

To investigate the functional significance of the observed CDS variations, we generated haplotype based three transgenic rice lines overexpressing *AhPDS1* (OE-*AhPDS1*^{LP1,2,3} and OE-*AhPDS1*^{SP1,3,7}) and confirmed strong induction of transgene expression in both (Figure 4a,b). Overexpression of the LP haplotype significantly increased grain length, width, and 1000 grain weight compared with wild-type plants, whereas overexpression of the SP haplotype produced no detectable changes in grain morphology (Figure 4c–h). We examined the cellular basis of this effect by analyzing mature grain epidermal tissues (Figure 4i). The number of cells per millimeter along the longitudinal axis was similar between OE-*AhPDS1*^{SP} and wild-type plants, while the OE-*AhPDS1*^{SP} was significantly less than that of the wild-type (Figure 4j). Consistently, the number of cells per square millimeter were similar (Figure 4k). In addition, cross-sections of central parts of the spikelet showed no significant difference in the total number of cells among OE-*AhPDS1*^{SP}, OE-*AhPDS1*^{LP} and wild-type lines (Figure 4l,m), but significantly enlarged cell size in OE-*AhPDS1*^{LP} plants (Figure 4n). These results indicated that *AhPDS1*^{LP} enhances grain yield not due to altered cell proliferation but by promoting cell expansion and simultaneously improving yield related traits.

Overexpression of *AhPDS1* enhances IAA biosynthesis via the indole-3-pyruvic acid (IPA) pathway in transgenic Arabidopsis

To further confirm the function of the *AhPDS1*, we also generated three transgenic *A. thaliana* lines overexpressing *AhPDS1* (OE-*AhPDS1*^{LP1,2,3} and OE-*AhPDS1*^{SP1,2,3}) (Figure 5a). Quantitative RT-PCR revealed that the overexpressed lines displayed markedly elevated transcript abundance relative to the wild-type (Col), with OE-*AhPDS1*^{LP1,2,3} lines exhibiting significantly higher expression than OE-*AhPDS1*^{SP1,2,3} lines (Figure 5b). Phenotypic analysis showed OE-*AhPDS1*^{LP} plants increased leaf length, leaf width, PL, and SL compared with wild-type plants, while OE-*AhPDS1*^{SP} plants did not show any significant differences among these traits when compared with the wild-type (Figure 5c–h). These findings suggest that the *AhPDS1* confer distinct functional effects on plant morphology, pod, and seed development. The overexpression of the LP allele appears to promote pod and seed size enlargement, whereas the SP allele does not induce similar phenotypic changes. This highlights the potential importance of sequence-specific regulatory mechanisms or protein function that drive the phenotypic divergence between the LP and SP genotypes, with the LP allele of *AhPDS1* playing a more prominent role in enhancing plant growth and yield traits.

Two biosynthetic pathways are known for IAA biosynthesis: the tryptophan (Trp)-dependent pathway and the Trp-independent pathway, which uses indole as a precursor. Therefore, to determine if *AhPDS1* overexpression enhances IAA biosynthesis in transgenic Arabidopsis, we analyzed the auxin spectrum in OE-*AhPDS1*^{LP} and wild-type plants using liquid chromatography–tandem mass spectrometry. The results showed significantly

higher levels of IAA and most IAA amino acid conjugates in OE-*AhPDS1*^{LP} compared with wild-type plants (Figure 5i; Table S4). Notably, levels of Trp, IPA, and IAA involved in the IPA pathway were significantly higher in OE-*AhPDS1*^{LP} plants, while other auxin metabolites from pathways such as IAOx-IAM-IAN (IAOx pathway) and TAM-IAAld (TAM pathway) were not significantly different or undetectable between OE-*AhPDS1*^{LP} and wild-type plants (Figure 5j). These findings suggest that *AhPDS1*, similar to the *YUC* family in other plants, participates in IAA biosynthesis through the IPA pathway. Previous studies have shown that the YUC family converts IPA to IAA in the IPA pathway, regulating various traits, such as plant height, flower size, fruit size, and seed size in different species (Cao et al., 2019; Luo & Di, 2023; Meng et al., 2023; Pérez Alonso, 2017; Ye et al., 2024; Zhao, 2012).

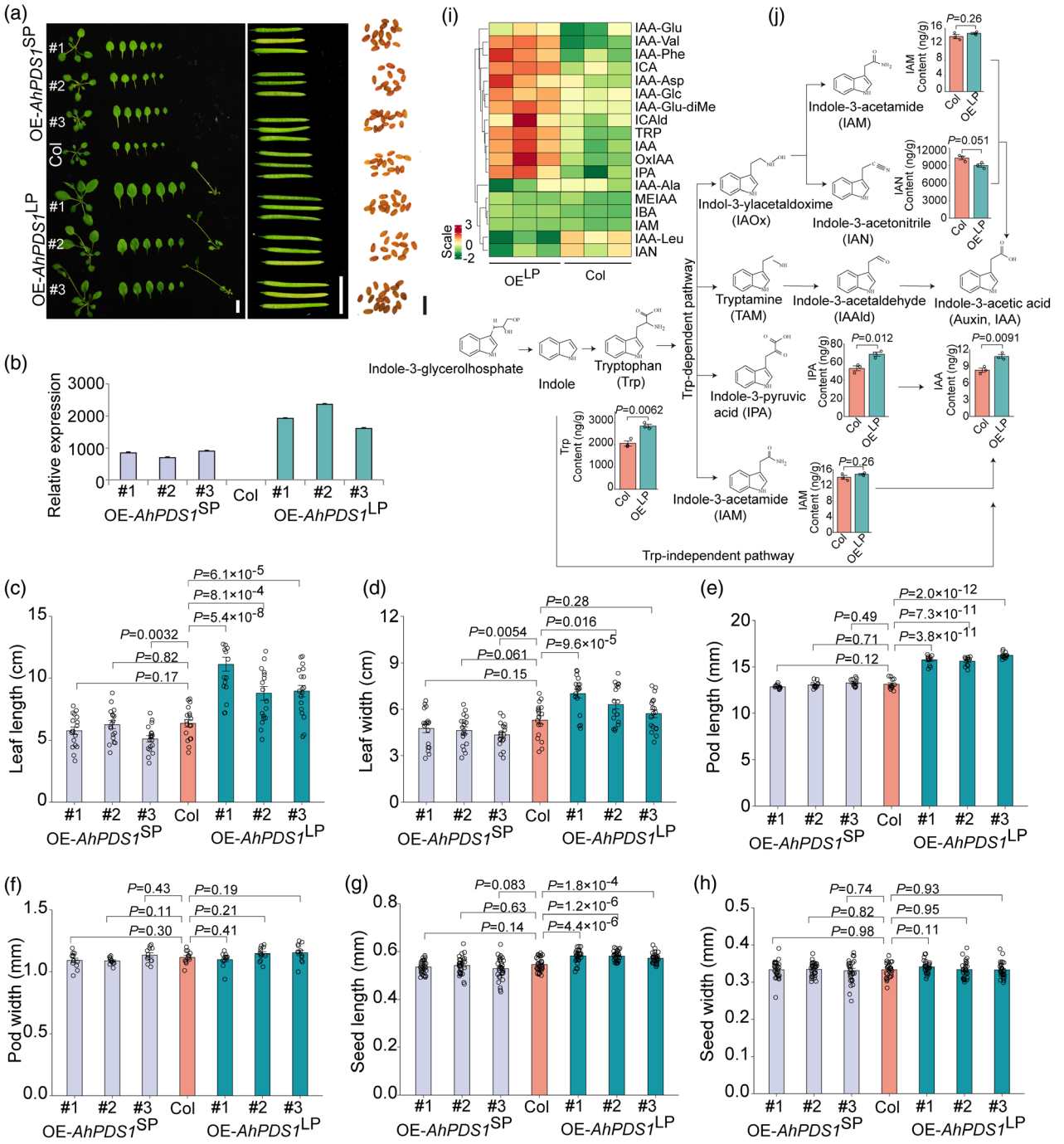

Figure 5. Overexpression of *AhPDS1* in *Arabidopsis thaliana* and its involvement in indole-3-acetic acid (IAA) biosynthesis via the indole-3-pyruvic acid pathway.
(a) Overexpression of *AhPDS1* in *A. thaliana*. This panel shows the phenotypic differences among overexpressed lines OE-*AhPDS1*^{LP1,2,3}, OE-*AhPDS1*^{SP1,2,3}, and wild-type (Col) plants. Overexpression of OE-*AhPDS1*^{LP} appears to influence leaf length, width, pod, and seed sizes. Left, middle and right scale bars = 1 cm, 1 cm, and 1 mm, respectively.
(b) Relative expression levels in overexpressed *AhPDS1* and wild-type (Col) lines.
(c–h) Comparative analysis of phenotypic traits in overexpressed *AhPDS1* and wild-type lines. Phenotypic traits include leaf length, leaf width, pod length, pod width, seed length, and seed width.
(i) Heatmap illustrating the content of IAA and related conjugates in OE-*AhPDS1*^{LP} and wild-type plants. The heatmap provides a comparative view of auxin levels, showing increased IAA and conjugates in overexpressed plants.
(j) Schematic overview of the IAA biosynthesis pathway with accompanying bar graphs, comparing the content of each biosynthetic intermediate in the overexpressed (OE-*AhPDS1*^{LP}) and wild-type plants. The higher levels of metabolites in the overexpressed lines suggest that *AhPDS1*^{LP} influences IAA biosynthesis, contributing to the observed phenotypic changes. Data in (b–h and j) are given as mean ± SE with three replications; n = 3, 18, 12, 30, and 3 independent samples for (b–h, and j), respectively. *P*-values were calculated by two-tailed Student's *t*-test.

Differential miRNA binding in the *AhPDS1* 3′ untranslated region (3′UTR) may underlie haplotype-specific transcript accumulation

To explore the molecular basis underlying the distinct expression levels of *AhPDS1* haplotypes observed in transgenic rice and Arabidopsis, we compared sequence variations between the LP and SP alleles and examined their potential effects on post-transcriptional regulation. Sequence alignment revealed multiple SNPs and one InDel (C/CU) within the 3′UTR of *AhPDS1* (Figure S8A). Because polymorphisms in 3′UTRs can influence transcript stability by altering microRNA (miRNA) binding affinity, we performed *in silico* miRNA target prediction using the psRNATarget platform (http://bioinformatics.psb.ugent.be/research). The analysis identified three peanut miRNAs with four potential binding sites within the *AhPDS1* 3′UTR (Figure S8B). Notably, the identified InDel (C/CU) overlapped with two of these predicted miRNA binding regions, suggesting that the SP allele may have altered miRNA-mRNA pairing efficiency compared with the LP allele. Such changes could reduce transcript stability or promote degradation of the SP derived mRNA, leading to its lower accumulation observed in heterologous expression systems. These findings provide a plausible molecular explanation for the haplotype specific expression differences of *AhPDS1*. Overall, the sequence variation in the 3′UTR, particularly the InDel affecting miRNA target sites, may contribute to differential post-transcriptional regulation between the LP and SP haplotypes.

DISCUSSION

Peanut pod size genetic mechanisms

Pod and seed size are among the most vital agronomic traits affecting crop yield, and their genetic regulation is both complex and multifactorial. Various QTLs and genes are involved in controlling pod size across different biological pathways. In most seed crops, the coordinated interaction between the embryo, endosperm, and testa determines the ultimate size of the pod and the seed (Bleckmann et al., 2014). In the context of genetic research, numerous studies have successfully uncovered the molecular mechanisms governing pod and seed size across various crops (Li et al., 2019). In peanut (*Arachis hypogaea*), advancements in this area have been achieved through techniques such as linkage mapping (Biswal et al., 2024; Guo et al., 2013; Kassie et al., 2023; Qin et al., 2012), association studies (Liu et al., 2022; Patel et al., 2022) and transcriptome analysis (Wu et al., 2022). The identified QTLs for pod and seed size traits have primarily been located on chromosomes A02, A05, A07, A09, B06, and B07 (Joshi et al., 2024; Kassie et al., 2023; Miao et al., 2023a, 2023b; Wang et al., 2018; Zhang et al., 2019). These findings are consistent with the association hotspots identified in this study (Figure S3; Table S1). Previous reports emphasized that pod and seed traits are typically polygenic, with multiple QTLs or genes contributing to their regulation (Liu et al., 2015). Genetic studies discovered overlapping genomic regions on chromosomes A05 and B05 that control both PW and SW (Gangurde et al., 2020; Lu, Liu, et al., 2018; Luo et al., 2017). In our analysis, several pleiotropic association hotspots were identified on different chromosomes (Table S1). Pleiotropic association hotspots on chromosomes A05 and B06 for pod and seed traits overlapped with previously reported QTLs (Gangurde et al., 2020). Notably, the hotspot B06.1, which governs both seed and pod size traits, was validated by multiple QTLs in biparental linkage mapping studies (Chavarro et al., 2020).

Subgenomic distribution of QTLs in peanut

Cultivated peanut is an allotetraploid species (AABB, $2n = 4\times = 40$), comprising two subgenomes that exhibit a high degree of homology. Due to this genetic complexity, most genes in peanut have multiple copies distributed within and across subgenomes. This leads to paired QTL distributions between the A and B subgenomes, a phenomenon supported by both previous research and our findings. For example, QTLs for SW have been shown to pair between chromosomes A05/B05, A06/B06, A07/B07,

and A09/B09 (Bertioli et al., 2016; Chen et al., 2019; Chen, Li, et al., 2016; Gangurde et al., 2020; Zheng et al., 2024). These paired associations were also observed in our study, particularly with the hotspots related to SW and PW on chromosomes A06/B06, further demonstrating the genetic parallelism between the subgenomes. The identification of these paired QTLs offers significant potential for peanut breeding, allowing for more precise elite gene selection from both subgenomes to accelerate the breeding of desirable pod and seed traits in future crop improvement efforts.

Role of *YUC* genes in seed development

Auxin biosynthesis plays a critical role in regulating plant growth and development, particularly in seed development. The *YUC* gene family is crucial for this process, with key members such as *YUC1*, *YUC2*, *YUC4*, and *YUC6* involved in auxin biosynthesis (Cheng et al., 2006; Yamamoto et al., 2007; Zhao et al., 2001). In strawberry (*Fragaria* spp.), *YUC* genes homologous to *AtYUC6* and *AtYUC4* have been implicated in flower and fruit development, further demonstrating their importance across plant species (Liu et al., 2012). Specifically, in cultivated strawberry, *FaYUC1* and *FaYUC2* play pivotal roles in the regulation of reproductive development. Similarly, in woodland strawberry, *FvYUC6* has been found to regulate both vegetative and reproductive development (Liu et al., 2014). In Arabidopsis, *AtYUC4* influences overall plant growth and development by modulating auxin biosynthesis and transport, and it plays a significant role in auxin-ABA interactions (Munguía-Rodríguez et al., 2020). The detailed role of YUC family genes for auxin biosynthesis in arabidopsis was reported earlier by (Mashiguchi et al., 2011). In peanuts two YUC genes, *arahy.WRP4Q5* (*YUC2*), *arahy.6PM354* (*YUC4*) involved in auxin biosynthesis were reported earlier by (Wu et al., 2022). Here, we identified *AhPDS1* on chromosome B06. It shows high homology to *AtYUC4*, a gene known to regulate seed size through auxin mediated pathways (Figure S6A,B). The structural modeling and stability analyses of *AhPDS1* (Figure S6C) provide mechanistic support for the observed haplotype specific functional divergence. The N402K substitution present in the SP haplotype is predicted to destabilize the YUC4-like enzyme by altering local cavity geometry and introducing a positively charged residue at a structurally sensitive position, potentially impairing substrate interaction or catalytic efficiency. Overexpression of *AhPDS1* in Arabidopsis and rice provided preliminary evidence supporting the role of this gene in regulating pod and seed sizes. Although these findings offer valuable insights, further research involving transgenic studies in peanut will be necessary to elucidate the precise function of *AhPDS1* in seed size regulation within the peanut genome.

IAA biosynthesis and its regulation in peanut

In plants, IAA biosynthesis is a critical process for growth regulation, primarily driven by multiple pathways. The *YUC* family of genes collaborates with *TAA1* (Tryptophan Aminotransferase of Arabidopsis) to catalyze the rate-limiting step of the IPA pathway, which converts Trp into IPA, and subsequently into IAA, a key auxin hormone (Mashiguchi et al., 2011; Tao et al., 2008). Four major biosynthetic pathways for IAA exist, which include the IAOx (*CYP79B*) pathway, the TAM pathway, the IPA (*YUC*) pathway, and the IAM pathway (Figure 5). Among these, the *YUC* pathway is of particular significance due to its role in converting IPA to IAA. Our study demonstrated that Arabidopsis plants overexpressing *AhPDS1* exhibited significantly elevated levels of Trp, IPA, and IAA compared with wild-type plants (Figure 5). These results suggest that *AhPDS1* in peanut may regulate IAA biosynthesis through the IPA pathway. However, while the IPA pathway appears to be the dominant route, the involvement of alternative pathways, such as the IAOx or IAM pathways, cannot be fully ignored and warrant further investigation.

Subcellular localization and GUS staining of *AhPDS1*

To further elucidate the function of *AhPDS1*, subcellular localization and GUS staining experiments were conducted. The subcellular localization analysis revealed that the *AhPDS1* protein is primarily localized to the cytoplasm consistent with its role in auxin biosynthesis. This localization pattern supports the hypothesis that *AhPDS1* participates in auxin production and transport within these cellular compartments. Additionally, GUS staining assay revealed that *AhPDS1* is expressed in multiple tissues, including roots and leaves (Figure 3e). The expression in these tissues indicates a potentially broad role for *AhPDS1* in plant growth and development, possibly influencing a range of physiological processes across different organ systems.

AhPDS1 appears to play a crucial role in regulating peanut pod development through its involvement in auxin biosynthesis, a hormone known to influence various growth processes. The differential expression of *AhPDS1* between LP and SP peanut genotypes, along with its impact on pod and seed size, highlights its significance in shaping key agronomic traits. The evidence from both expression and functional studies in arabidopsis and rice suggests that *AhPDS1* contributes to pod expansion, likely by modulating cell division and elongation within pod tissues. This makes *AhPDS1* a promising target for breeding programs aimed at improving peanut yield and pod size, as manipulating its expression or activity could enhance these desirable traits in cultivated peanut varieties. Further studies exploring its precise molecular mechanisms will be

essential to fully understand how *AhPDS1* influences pod development and other related physiological processes in peanuts.

CONCLUSIONS

Our findings advance current knowledge of the genetic and molecular mechanisms underlying seed size regulation in peanut. The identification of QTL hotspots, the elucidation of subgenomic distributions, and the functional characterization of the *AhPDS1*, contribute to the growing body of knowledge on peanut seed and pod development. The discovery that *AhPDS1* regulates IAA biosynthesis via the IPA pathway and its localization to the cytoplasm reinforces its central role in seed size determination. These insights have significant implications for future peanut breeding programs aimed at improving seed and pod traits, offering new avenues for crop improvement through targeted genetic manipulation. Further exploration of the molecular pathways and genetic interactions involved in seed development will continue to enhance our understanding of the complex traits that govern peanut yield and quality.

METHODS

Plant materials and phenotyping

The association mapping population in this study comprises 390 peanut accessions collected from 15 countries or regions worldwide. Detailed information regarding the origin, population structure, and genetic diversity of these accessions has been previously documented (Lu, Huang, Liu, Garg, Gangurde, Li, Chitikineni, Guo, Pandey, Li, Wang, et al., 2024). All accessions were cultivated in the experimental field located in Guangzhou, China (113.28° E and 23.12° N), under four distinct environments in the early and late seasons in both 2017 and 2018. The experiment was conducted using a randomized complete block design, with three replicates for each accession. Each plot consisted of a grid measuring six columns by six rows, with individual plants spaced ~10 cm apart to ensure adequate separation. Four pod and seed size traits, specifically PL, PW, PT, HPW, SL, SW, ST, and HSW were measured in each environment after harvest. The detailed methodology for these measurements has also been previously described (Lu, Huang, Liu, Garg, Gangurde, Li, Chitikineni, Guo, Pandey, Li, Wang, et al., 2024).

Genotyping and association mapping and *in silico* structural and stability prediction of *AhPDS1* haplotypes

Each accession was resequenced at an approximate depth of 10× using the Illumina HiSeq X-ten platform. Detailed sequencing protocols followed those previously reported by Lu, Huang, Liu, Garg, Gangurde, Li, Chitikineni, Guo, Pandey, Li, Wang, et al. (2024). A total of 2 564 993 SNPs with a minor allele frequency (MAF) of ≥0.05 were utilized for genome-wide association mapping. The Efficient Mixed-Model Association eXpedited (EMMAX) method was employed for the association mapping analysis, incorporating the top three principal components (PCs) and the relative kinship matrix as covariates to account for population structure and relatedness. The significance threshold for associations was set at $P = 1.0E\text{-}06$, as estimated by Bonferroni correction (Moran, 2003; Nakagawa, 2004). To identify LD blocks associated with significant SNPs, the LDheatmap package (Shin et al., 2006) in R (https://www.r-project.org/) was used. To assess the potential functional consequences of the non-synonymous N402K substitution in *AhPDS1*, a series of computational analyses were performed integrating sequence conservation, structural modeling, and stability prediction. The three-dimensional (3D) structure of *AhPDS1* was modeled using Missense3D (https://missense3d.bc.ic.ac.uk/), which evaluates structural impacts of amino acid substitutions based on homology-modeled templates. Structural effects were visualized to identify changes in local geometry and cavity features between the LP (wild-type) and SP (mutant) haplotypes. Protein stability changes resulting from the N402K substitution were estimated using I-Mutant 2.0 (https://folding.biofold.org/i-mutant/i-mutant2.0.html) and MutPro (http://bioinfo.unipune.ac.in/MutPro/), both of which predict the direction and magnitude of free energy (ΔΔG) alterations upon mutation. Additionally, Project HOPE (https://www3.cmbi.umcn.nl/hope/) was employed to evaluate the biochemical consequences of residue substitution, including changes in charge, polarity, and steric compatibility within the local structural environment.

Identification of candidate genes and expression dynamics

Candidate genes were identified within a LD block region, using the reference genome 'Fuhuasheng' (Chen et al., 2019) to predict their putative functions. RNA-seq datasets (Haifen Li, unpublished) provided preliminary insights into the expression levels of these candidate genes. To further validate the expression levels, quantitative real-time PCR (qRT-PCR) was conducted. Total RNA was extracted from plant samples using the Plant RNA Extraction Kit (TIANGEN, Beijing, China) and reverse transcribed into cDNA using the PrimeScript RT reagent Kit (Takara, Dalian, China) according to the manufacturer's instructions. The qRT-PCR was performed on an Applied Biosystems Viia7 Real-Time PCR system using SYBR Green Master Mix (YEASEN, Shanghai, China). Each sample was analyzed in triplicate to ensure accuracy and reliability. The qRT-PCR cycling conditions were as follows: an initial incubation at 95°C for 5 min, followed by 40 cycles of amplification (95°C for 10 sec and 60°C for 30 sec). The comparative $2^{-\Delta\Delta Ct}$ method (Pfaffl, 2001) was employed to evaluate the relative expression levels of the candidate genes.

Overexpression of *AhPDS1* in *A. thaliana* and rice

Total RNA was extracted from 2-week-old peanut seedlings and subsequently reverse transcribed into cDNA. Using this cDNA as a template, the full-length CDS of the target gene was amplified by PCR. The resulting PCR fragment was then inserted into the pGEOEP35S-H-GFP vector to enable overexpression analysis, driven by the cauliflower mosaic virus 35S promoter. All plasmid constructs were introduced into *Agrobacterium tumefaciens* strain GV3101 and subsequently transferred into *A. thaliana* (Columbia ecotype) and *japonica* variety Nipponbare. The T_4 generations of transgenic plants were used for phenotypic analysis. Seeds of these Arabidopsis plants were photographed and measured using an anatomical microscope equipped with a 1× objective lens and a 10× eyepiece lens (Mshot, Guangzhou, China). Detailed sequences of all primers used in this study are provided in Table S5. This method ensured the reliable generation of overexpressed transgenic lines, enabling a thorough examination of the phenotypic consequences of target gene overexpression.

Quantification of auxin spectrum in overexpressed Arabidopsis plants

The concentration of endogenous auxin was determined through a protocol performed by Metware (Wuhan, China). Fresh rice tissues were harvested, weighed, rapidly frozen in liquid nitrogen, and stored at −70°C. Plant material (120 mg fresh weight) was pulverized under liquid nitrogen and extracted using a methanol/water solution (8:2) at 4°C. The extracts were centrifuged at 12 000× ***g*** for 15 min at 4°C. The resulting supernatant was evaporated to dryness under a nitrogen gas stream and reconstituted in methanol/water (3:7). After a final centrifugation step, the supernatant was analyzed using a liquid chromatography-electrospray ionization tandem mass spectrometry system (Dong et al., 2020).

The promoter activity of *AhPDS1* via GUS in transgenic plants

The native promoter of *AhPDS1* was synthesized and cloned into the pCAMBIA1391-GUS vector by Sangon Biotech Co., Ltd. (Shanghai, China). To assess promoter activity, *AhPDS1*-promoter transgenic plants were generated. Plant tissues were initially incubated in a phosphate buffer (50 mM Na_2HPO_4, 50 mM NaH_2PO_4) containing 0.5 mM $K_3Fe(CN)_6$ and 0.5 mM $K_4Fe(CN)_6{\cdot}3H_2O$ for 5 min. Following this, tissues were transferred to a GUS staining solution consisting of the same phosphate buffer supplemented with 10 mM EDTA Na_2, 1% Triton-100, and 2 mM X-Gluc, and incubated for 12 h at 37°C. Post incubation, the tissues were decolorized by washing with 95% ethanol at 65°C over a period of 12 h. The stained tissues were subsequently examined under a stereomicroscope (Leica DVM6) to visualize GUS expression patterns (Dedow et al., 2022).

Subcellular localization of *AhPDS1*-GFP fusion protein and histological observations

The subcellular localization of the *AhPDS1*-GFP fusion protein was studied using a transient expression system in leaf cell protoplasts, facilitated by Wuhan Edgene Bio-Tech Co., Ltd. (Wuhan, China). Arabidopsis leaves from 3-week-old plants were enzymatically digested using a solution containing 1.5% Cellulase R10, 0.75% Macerozyme R10, 600 mM mannitol, 10 mM MES (pH 5.7), and 0.04% 2-hydroxy-1-ethanethiol. The digestion process was carried out under vacuum for 3 h at 23°C. Protoplasts were isolated by filtration through 40-μm nylon mesh and centrifugation at 400 ***g*** for 5 min at 4°C. After discarding the supernatant, the protoplasts were washed twice with cold W5 solution (154 mM NaCl, 125 mM $CaCl_2$, 2 mM KH_2PO_4, 2 mM MES, pH 5.7) and then resuspended in MMG solution (400 mM mannitol, 15 mM $MgCl_2{\cdot}6H_2O$, 4 mM MES, pH 5.7). Approximately, 20–40 protoplasts per field of view were observed under 40× magnification. The *AhPDS1* CDS was cloned into the pEGOEP35S-H-GFP vector and transformed into protoplasts derived from Col-0 and *AhPDS1*-OE plants. For transformation, 10 μl of the plasmid DNA was mixed with 100 μl of protoplasts and 110 μl of 40% PEG4000 solution, followed by incubation in a 22.5°C water bath for 15–20 min. The reaction was halted by adding W5 solution, and the protoplasts were centrifuged at 400 ***g*** for 5 min at 4°C. After washing twice with cold W5 solution, the protoplasts were incubated overnight at 23°C under low light. The subcellular localization of *AhPDS1*-GFP was then visualized using a laser confocal microscope (Olympus FV3000) at an excitation wavelength of 488 nm and an emission wavelength of 510–530 nm. Localization was further examined in 10-day-old transgenic plants treated with 300 mM mannitol under varying photoperiods, with GFP signals captured using the same confocal microscope (Cheng et al., 2011; Rolland, 2018). The outer surface of the lemma from mature rice seeds was observed with a scanning electron microscope at an acceleration voltage of 15 kV. Cell number and cell density were calculated along the longitudinal axis (Si et al., 2016).

Exogenous application of hormones on peanut

Peanut genotypes LP and SP were grown in cylindrical plastic pots (30 cm diameter × 26 cm height) filled with a soil mixture of coarse sand, laterite, and paddy field soil (4:4:1, v/v/v). Three seeds were sown per pot, and plants were maintained under standard field management practices. Hormone treatments were prepared by dissolving IAA, TIBA, and NPA in dimethyl sulfoxide (DMSO) at 0.1 mol L^{-1}. A DMSO-only solution served as the control (CK) (Peng et al., 2013). Working solutions of IAA, NPA, and TIBA (1×10^{-5} mol L^{-1}) were applied as foliar sprays. To avoid contamination of the soil, the base of each plant was covered with a thin transparent plastic film during spraying, which was removed the following morning. Each treatment consisted of four pots, and the experiment followed a completely randomized design with three replicates.

Statistical analyses

The statistical analyses were conducted using R software (version 4.2.0). To evaluate differences in gene expression levels, phenotypic traits, and IAA content between two sample groups, a two-tailed Student's *t*-test was performed. This analysis was implemented using the ggsignif package in R (Ahlmann-Eltze & Patil, 2021).

AUTHOR CONTRIBUTIONS

QL: Writing—original draft, Formal analysis, Resources. MJU: Writing—original draft, Formal analysis. HL: Investigation. HL: Writing—review. RW: Writing—review and editing. LH: Formal Analysis. QY: Writing—review and editing. MKP: Writing—review. RKV: Writing—review. XC: Resources. YH: Resources, Writing—editing.

ACKNOWLEDGMENTS

This work was supported by the National Natural Science Foundation of China (32172051 and 32301869), the National Key R&D Program of China (2023YFD1202800), China Agriculture Research System of MOF and MARA (CARS-13), the Open Competition Program of Top Ten Critical Priorities of Agricultural Science and Technology Innovation for the 14th Five-Year Plan in Guangdong Province (2022SDZG05), Guangdong Provincial Key Research and Development Program-Modern Seed Industry (2022B0202060004), Guangdong Science and Technology Plan Project (2023B1212060038), Guangdong Basic and Applied Basic Research Foundation (2023A1515010098), the Special Support Program of Guangdong Province (2021TX06N789), Guangzhou Basic and Applied Basic Research Foundation (202201010281 and 2023A04J0776), Special Fund for High Level Academy of Agriculture Science (R2020PY-JX004, R2020PY-JG005, R2021PY-QY003, R2022YJ-YB3025 and R2023PY-JG007), the Foundation of Director of Crop Research Institute of Guangdong Academy of Agriculture Sciences (202101, 202201 and 202306), the Project of Collaborative Innovation Center of GDAAS (XTXM202203).

CONFLICT OF INTEREST

The authors declare that the research was conducted in the absence of any commercial or financial relationships that could be construed as a potential conflict of interest.

DATA AVAILABILITY STATEMENT

All the 390 genomic sequence data for GWAS analysis has been shown in our previous study (Lu, Huang, Liu, Garg, Gangurde, Li, Chitikineni, Guo, Pandey, Li, Wang, et al., 2024).

SUPPORTING INFORMATION

Additional Supporting Information may be found in the online version of this article.

Figure S1. Local Manhattan plots for the significant associations for eight pod and seed size-related traits across four different environments.

Figure S2. Density of significant SNPs across the A (At) and B (Bt) subgenomes of the peanut.

Figure S3. Distribution of significant SNPs and association hotspots within the peanut genome.

Figure S4. Venn diagram of the number of significant SNPs repeatedly identified in multiple environments.

Figure S5. Expression profiles of 10 candidate genes (I–X; listed in Table S3) in seeds (A) and shells (B) of small-pod ('s') and large-pod ('L') peanut varieties across five developmental stages (1–5).

Figure S6. (A) Homologous analysis of the candidate gene *Ahy_B06g085516* across cultivated peanut genomes and related species, showing sequence conservation and gene structure variation. (B) Phylogenetic relationships and sequence alignment of *Ahy_B06g085516* (*AhPDS1*) with homologs from Arabidopsis, highlighting evolutionary conservation that support its potential role in pod and seed size regulation. (C) *In silico* structural and stability analyses of the AhPDS1/YUC4 N402K substitution.

Figure S7. Amino acid changes between the LP (large pod) and SP (small pod) genotypes.

Figure S8. Effects of exogenous IAA and auxin transport inhibitors (NPA and TIBA) on pod morphology in contrasting peanut genotypes.

Figure S9. Predicted miRNA binding sites within the *AhPDS1* 3′UTR.

Table S1. Identification of hotspot associations for pod and seed size related traits.

Table S2. Significant SNPs identified in multiple environments.

Table S3. Identification of prediction genes on hotspot B06.1 and their expression levels.

Table S4. Analysis of auxin spectrum between the wild type and overexpression plants with LP genotype.

Table S5. Primer used in this study.

REFERENCES

Ahlmann-Eltze, C. & **Patil, I.** (2021) *ggsignif: R package for displaying significance brackets for 'ggplot2'*.

Bertioli, D.J., **Cannon, S.B.**, **Froenicke, L.**, **Huang, G.**, **Farmer, A.D.**, **Cannon, E.K.S.** ***et al.*** (2016) The genome sequences of *Arachis duranensis* and *Arachis ipaensis*, the diploid ancestors of cultivated peanut. *Nature Genetics*, **48**(4), 438–446.

Bertioli, D.J., **Jenkins, J.**, **Clevenger, J.**, **Dudchenko, O.**, **Gao, D.**, **Seijo, G.** ***et al.*** (2019) The genome sequence of segmental allotetraploid peanut *Arachis hypogaea*. *Nature Genetics*, **51**(5), 877–884.

Biswal, A.K., **Ozias-Akins, P.** & **Holbrook, C.C.** (2024) Recent technological advancements for identifying and exploiting novel sources of Pest and disease resistance for Peanut improvement. *Agronomy*, **14**(12), 3071.

Bleckmann, A., **Alter, S.** & **Dresselhaus, T.** (2014) The beginning of a seed: regulatory mechanisms of double fertilization. *Frontiers in Plant Science*, **5**, 452.

Campanelli, G., **Sestili, S.**, **Acciarri, N.**, **Montemurro, F.**, **Palma, D.**, **Leteo, F.** ***et al.*** (2019) Multi-parental advances generation inter-cross population, to develop organic tomato genotypes by participatory plant breeding. *Agronomy*, **9**(3), 119.

Cao, X., **Yang, H.**, **Shang, C.**, **Ma, S.**, **Liu, L.** & **Cheng, J.** (2019) The roles of auxin biosynthesis YUCCA gene family in plants. *International Journal of Molecular Sciences*, **20**(24), 6343.

Chavarro, C., **Chu, Y.**, **Holbrook, C.**, **Isleib, T.**, **Bertioli, D.**, **Hovav, R.** ***et al.*** (2020) Pod and seed trait QTL identification to assist breeding for peanut market preferences. *G3: Genes, Genomes, Genetics*, **10**(7), 2297–2315.

Chen, W., **Jiao, Y.**, **Cheng, L.**, **Huang, L.**, **Liao, B.**, **Tang, M.** ***et al.*** (2016) Quantitative trait locus analysis for pod-and kernel-related traits in the cultivated peanut (*Arachis hypogaea* L.). *BMC Genetics*, **17**, 1–9.

Chen, W., **Yue, Y.**, **Chen, C.**, **Yang, J.**, **Chen, Y.** & **Zhang, H.** (2025) Genome-wide association studies revealed genetic loci and candidate genes for pod-related traits in peanut. *Plant Molecular Biology Reporter*, **43**(2), 766–776.

Chen, X., **Li, H.**, **Pandey, M.K.**, **Yang, Q.**, **Wang, X.**, **Garg, V.** ***et al.*** (2016) Draft genome of the peanut A-genome progenitor (*Arachis duranensis*) provides insights into geocarpy, oil biosynthesis, and allergens. *Proceedings of the National Academy of Sciences*, **113**(24), 6785–6790.

Chen, X., **Lu, Q.**, **Liu, H.**, **Zhang, J.**, **Hong, Y.**, **Lan, H.** ***et al.*** (2019) Sequencing of cultivated peanut, *Arachis hypogaea*, yields insights into genome evolution and oil improvement. *Molecular Plant*, **12**(7), 920–934.

Cheng, W., **Zhang, H.**, **Zhou, X.**, **Liu, H.**, **Liu, Y.**, **Li, J.** ***et al.*** (2011) Subcellular localization of rice hexokinase (OsHXK) family members in the mesophyll protoplasts of tobacco. *Biologia Plantarum*, **55**, 173–177.

Cheng, Y., **Dai, X.** & **Zhao, Y.** (2006) Auxin biosynthesis by the YUCCA flavin monooxygenases controls the formation of floral organs and vascular tissues in Arabidopsis. *Genes & Development*, **20**(13), 1790–1799.

de Blas, F.J., **Bruno, C.**, **Arias, R.**, **Ballén-Taborda, C.**, **Mamaní, E.M.C.**, **Oddino, C.** ***et al.*** (2021) Genetic mapping and QTL analysis for peanut smut resistance. *BMC Plant Biology*, **21**, 1–15.

Dedow, L.K., **Oren, E.** & **Braybrook, S.A.** (2022) Fake news blues: a GUS staining protocol to reduce false-negative data. *Plant Direct*, **6**(2), e367.

Dong, N.-Q., **Sun, Y.**, **Guo, T.**, **Shi, C.L.**, **Zhang, Y.M.**, **Kan, Y.** ***et al.*** (2020) UDP-glucosyltransferase regulates grain size and abiotic stress tolerance associated with metabolic flux redirection in rice. *Nature Communications*, **11**(1), 2629.

Fragoso, C.A., **Moreno, M.**, **Wang, Z.**, **Heffelfinger, C.**, **Arbelaez, L.J.**, **Aguirre, J.A.** ***et al.*** (2017) Genetic architecture of a rice nested association mapping population. *G3: Genes, Genomes, Genetics*, **7**(6), 1913–1926.

Gangurde, S.S., **Pasupuleti, J.**, **Parmar, S.**, **Variath, M.T.**, **Bomireddy, D.**, **Manohar, S.S.** ***et al.*** (2023) Genetic mapping identifies genomic regions and candidate genes for seed weight and shelling percentage in groundnut. *Frontiers in Genetics*, **14**, 1128182.

Gangurde, S.S., **Wang, H.**, **Yaduru, S.**, **Pandey, M.K.**, **Fountain, J.C.**, **Chu, Y.** ***et al.*** (2020) Nested-association mapping (NAM)-based genetic dissection uncovers candidate genes for seed and pod weights in peanut (*Arachis hypogaea*). *Plant Biotechnology Journal*, **18**(6), 1457–1471.

Guo, B., **Pandey, M.K.**, **He, G.**, **Zhang, X.**, **Liao, B.**, **Culbreath, A.** ***et al.*** (2013) Recent advances in molecular genetic linkage maps of cultivated peanut. *Peanut Science*, **40**(2), 95–106.

Huang, L., **He, H.**, **Chen, W.**, **Ren, X.**, **Chen, Y.**, **Zhou, X.** ***et al.*** (2015) Quantitative trait locus analysis of agronomic and quality-related traits in cultivated peanut (*Arachis hypogaea* L.). *Theoretical and Applied Genetics*, **128**, 1103–1115.

Huang, R., **Li, H.**, **Gao, C.**, **Yu, W.** & **Zhang, S.** (2023) Advances in omics research on peanut response to biotic stresses. *Frontiers in Plant Science*, **14**, 1101994.

Jha, S., **Quaiyum, Z.**, **Prasad, B.D.**, **Sahni, S.**, **Mandyal, S.S.**, **Singh, A.** ***et al.*** (2025) Meta-QTL analysis, candidate gene identification, and validation

by GWAS for agronomic traits and stress tolerance in pea (*Pisum sativum* L.). *Plant Biotechnology Reports*, **19**, 481–514.

Joshi, P., **Soni, P.**, **Sharma, V.**, **Manohar, S.S.**, **Kumar, S.**, **Sharma, S.** ***et al.*** (2024) Genome-wide mapping of quantitative trait loci for yield-attributing traits of Peanut. *Genes*, **15**(140), 2024.

Kassie, F.C., **Nguepjop, J.R.**, **Ngalle, H.B.**, **Assaha, D.V.M.**, **Gessese, M.K.**, **Abtew, W.G.** ***et al.*** (2023) An overview of mapping quantitative trait loci in peanut (*Arachis hypogaea* L.). *Genes*, **14**(6), 1176.

Leal-Bertioli, S.C., **Moretzsohn, M.C.**, **Santos, S.P.**, **Brasileiro, A.C.**, **Guimarães, P.M.**, **Bertioli, D.J.** ***et al.*** (2017) Phenotypic effects of allotetraploidization of wild *Arachis* and their implications for peanut domestication. *American Journal of Botany*, **104**(3), 379–388.

Li, N., **Xu, R.** & **Li, Y.** (2019) Molecular networks of seed size control in plants. *Annual Review of Plant Biology*, **70**(1), 435–463.

Liu, H., **Xie, W.F.**, **Zhang, L.**, **Valpuesta, V.**, **Ye, Z.W.**, **Gao, Q.H.** ***et al.*** (2014) Auxin biosynthesis by the YUCCA6 flavin monooxygenase gene in woodland strawberry. *Journal of Integrative Plant Biology*, **56**(4), 350–363.

Liu, H., **Ying, Y.Y.**, **Zhang, L.**, **Gao, Q.H.**, **Li, J.**, **Zhang, Z.** ***et al.*** (2012) Isolation and characterization of two YUCCA flavin monooxygenase genes from cultivated strawberry (*Fragaria* × *ananassa* Duch.). *Plant Cell Reports*, **31**, 1425–1435.

Liu, J., **Hua, W.**, **Hu, Z.**, **Yang, H.**, **Zhang, L.**, **Li, R.** ***et al.*** (2015) Natural variation in ARF18 gene simultaneously affects seed weight and silique length in polyploid rapeseed. *Proceedings of the National Academy of Sciences of the United States of America*, **112**(37), E5123–E5132.

Liu, Y., **Shao, L.**, **Zhou, J.**, **Li, R.**, **Pandey, M.K.**, **Han, Y.** ***et al.*** (2022) Genomic insights into the genetic signatures of selection and seed trait loci in cultivated peanut. *Journal of Advanced Research*, **42**, 237–248.

López-Bellido, F., **López-Bellido, L.** & **López-Bellido, R.** (2005) Competition, growth and yield of faba bean (*Vicia faba* L.). *European Journal of Agronomy*, **23**(4), 359–378.

Lu, Q., **Hong, Y.**, **Li, S.**, **Liu, H.**, **Li, H.**, **Zhang, J.** ***et al.*** (2019) Genome-wide identification of microsatellite markers from cultivated peanut (*Arachis hypogaea* L.). *BMC Genomics*, **20**, 1–9.

Lu, Q., **Huang, L.**, **Liu, H.**, **Garg, V.**, **Gangurde, S.S.**, **Li, H.** ***et al.*** (2024) A genomic variation map provides insights into peanut diversity in China and associations with 28 agronomic traits. *Nature Genetics*, **56**(3), 530–540.

Lu, Q., **Huang, L.**, **Liu, H.**, **Garg, V.**, **Gangurde, S.S.**, **Li, H.** ***et al.*** (2024) A genomic variation map provides insights into peanut diversity in China and associations with 28 agronomic traits. *Nature Genetics*, **56**, 1–540.

Lu, Q., **Li, H.**, **Hong, Y.**, **Zhang, G.**, **Wen, S.**, **Li, X.** ***et al.*** (2018) Genome sequencing and analysis of the peanut B-genome progenitor (*Arachis ipaensis*). *Frontiers in Plant Science*, **9**, 604.

Lu, Q., **Liu, H.**, **Hong, Y.**, **Li, H.**, **Liu, H.**, **Li, X.** ***et al.*** (2018) Consensus map integration and QTL meta-analysis narrowed a locus for yield traits to 0.7 cm and refined a region for late leaf spot resistance traits to 0.38 cm on linkage group A05 in peanut (*Arachis hypogaea* L.). *BMC Genomics*, **19**, 1–10.

Luo, H., **Ren, X.**, **Li, Z.**, **Xu, Z.**, **Li, X.**, **Huang, L.** ***et al.*** (2017) Co-localization of major quantitative trait loci for pod size and weight to a 3.7 cm interval on chromosome A05 in cultivated peanut (*Arachis hypogaea* L.). *BMC Genomics*, **18**, 1–12.

Luo, P. & **Di, D.-W.** (2023) Precise regulation of the TAA1/TAR-YUCCA auxin biosynthesis pathway in plants. *International Journal of Molecular Sciences*, **24**(10), 8514.

Mashiguchi, K., **Tanaka, K.**, **Sakai, T.**, **Sugawara, S.**, **Kawaide, H.**, **Natsume, M.** ***et al.*** (2011) The main auxin biosynthesis pathway in Arabidopsis. *Proceedings of the National Academy of Sciences*, **108**(45), 18512–18517.

Meijie, L., **Zhang, Y.**, **Chen, K.**, **Kong, M.**, **Song, W.**, **Lu, B.** ***et al.*** (2019) Mapping of quantitative trait loci for seedling salt tolerance in maize. *Molecular Breeding*, **39**, 1–12.

Meng, S., **Xiang, H.**, **Yang, X.**, **Ye, Y.**, **Ma, Y.**, **Han, L.** ***et al.*** (2023) Analysis of YUC and TAA/TAR gene families in tomato. *Horticulturae*, **9**(6), 665.

Miao, P., **Meng, X.**, **Li, Z.**, **Sun, S.**, **Chen, C.Y.** & **Yang, X.** (2023a) Mapping quantitative trait loci (QTLs) for hundred-pod and hundred-seed weight under seven environments in a recombinant inbred line population of cultivated peanut (*Arachis hypogaea* L.). *Genes*, **14**(9), 1792.

Miao, P., **Meng, X.**, **Li, Z.**, **Sun, S.**, **Chen, C.Y.** & **Yang, X.** (2023b) Mapping quantitative trait locus (QTLs) for hundred pod and seed weight under seven environments in a RIL cultivated Peanut (*Arachis hypogaea* L.) population. *Genes (Basel)*, **14**, 1792.

Moran, M.D. (2003) Arguments for rejecting the sequential Bonferroni in ecological studies. *Oikos*, **100**(2), 403–405.

Munguía-Rodríguez, A.G., **López-Bucio, J.S.**, **Ruiz-Herrera, L.F.**, **Ortiz-Castro, R.**, **Guevara-García, Á.A.**, **Marsch-Martínez, N.** ***et al.*** (2020) YUCCA4 overexpression modulates auxin biosynthesis and transport and influences plant growth and development via crosstalk with abscisic acid in *Arabidopsis thaliana*. *Genetics and Molecular Biology*, **43**(1), e20190221.

Nakagawa, S. (2004) A farewell to Bonferroni: the problems of low statistical power and publication bias. *Behavioral Ecology*, **15**(6), 1044–1045.

Pandey, M.K., **Agarwal, G.**, **Kale, S.M.**, **Clevenger, J.**, **Nayak, S.N.**, **Sriswathi, M.** ***et al.*** (2017) Development and evaluation of a high density genotyping 'Axiom_arachis' array with 58 K SNPs for accelerating genetics and breeding in groundnut. *Scientific Reports*, **7**(1), 40577.

Patel, J.D., **Wang, M.L.**, **Dang, P.**, **Butts, C.**, **Lamb, M.** & **Chen, C.Y.** (2022) Insights into the genomic architecture of seed and pod quality traits in the US peanut mini-core diversity panel. *Plants*, **11**(7), 837.

Peng, Q., **Wang, H.**, **Tong, J.**, **Kabir, M.H.**, **Huang, Z.** & **Xiao, L.** (2013) Effects of indole-3-acetic acid and auxin transport inhibitor on auxin distribution and development of peanut at pegging stage. *Scientia Horticulturae*, **162**, 76–81.

Pérez Alonso, M.M. (2017) In-depth analysis of jasmonate-mediated indole-3-acetic acid (IAA) biosynthesis and its implication in plant development. Thesis (Doctoral), E.T.S. de Ingeniería Agronómica, Alimentaria y de Biosistemas (UPM). https://doi.org/10.20868/UPM.thesis.47133

Pfaffl, M.W. (2001) A new mathematical model for relative quantification in real-time RT–PCR. *Nucleic Acids Research*, **29**(9), e45.

Qin, H., **Feng, S.**, **Chen, C.**, **Guo, Y.**, **Knapp, S.**, **Culbreath, A.** ***et al.*** (2012) An integrated genetic linkage map of cultivated peanut (*Arachis hypogaea* L.) constructed from two RIL populations. *Theoretical and Applied Genetics*, **124**(4), 653–664.

Raza, A., **Chen, H.**, **Zhang, C.**, **Zhuang, Y.**, **Sharif, Y.**, **Cai, T.** ***et al.*** (2024) Designing future peanut: the power of genomics-assisted breeding. *Theoretical and Applied Genetics*, **137**(3), 66.

Robledo, G., **Lavia, G.** & **Seijo, G.** (2009) Species relations among wild *Arachis* species with the A genome as revealed by FISH mapping of rDNA loci and heterochromatin detection. *Theoretical and Applied Genetics*, **118**(7), 1295–1307.

Rolland, V. (2018) Determining the subcellular localization of fluorescently tagged proteins using protoplasts extracted from transiently transformed *Nicotiana benthamiana* leaves. In *Photosynthesis*. Methods in Molecular Biology (Covshoff, S. ed). New York, NY: Humana Press, Vol **1770**.

Seijo, G., **Lavia, G.I.**, **Fernández, A.**, **Krapovickas, A.**, **Ducasse, D.A.**, **Bertioli, D.J.** ***et al.*** (2007) Genomic relationships between the cultivated peanut (*Arachis hypogaea*, Leguminosae) and its close relatives revealed by double GISH. *American Journal of Botany*, **94**(12), 1963–1971.

Sharma, A. & **Chahota, R.K.** (2025) Genome-wide association studies for identification of novel QTLs related to agronomic traits in Horsegram (*Macrotyloma uniflorum*). *Plant Molecular Biology Reporter*, **43**(2), 379–391.

Shin, J.-H., **Blay, S.**, **Graham, J.** & **McNeney, B.** (2006) LDheatmap: an R function for graphical display of pairwise linkage disequilibria between single nucleotide polymorphisms. *Journal of Statistical Software*, **16**, 1–9.

Shirasawa, K., **Koilkonda, P.**, **Aoki, K.**, **Hirakawa, H.**, **Tabata, S.**, **Watanabe, M.** ***et al.*** (2012) In silico polymorphism analysis for the development of simple sequence repeat and transposon markers and construction of linkage map in cultivated peanut. *BMC Plant Biology*, **12**, 1–13.

Shirasawa, S., **Endo, T.**, **Nakagomi, K.**, **Yamaguchi, M.** & **Nishio, T.** (2012) Delimitation of a QTL region controlling cold tolerance at booting stage of a cultivar,'Lijiangxintuanheigu', in rice, *Oryza sativa* L. *Theoretical and Applied Genetics*, **124**, 937–946.

Si, L., **Chen, J.**, **Huang, X.**, **Gong, H.**, **Luo, J.**, **Hou, Q.** ***et al.*** (2016) OsSPL13 controls grain size in cultivated rice. *Nature Genetics*, **48**(4), 447–456.

Smartt, J., **Gregory, W.** & **Gregory, M.P.** (1978) The genomes of *Arachis hypogaea*. 1. Cytogenetic studies of putative genome donors. *Euphytica*, **27**(3), 665–675.

Sun, H., **Ren, L.**, **Qi, F.**, **Wang, H.**, **Yu, S.**, **Sun, Z.** ***et al.*** (2022) BSA-seq approach identified candidate region and diagnostic marker for chilling tolerance of high oleic acid peanut at germination stage. *Agronomy*, **13**(1), 18.

Tao, Y., **Ferrer, J.L.**, **Ljung, K.**, **Pojer, F.**, **Hong, F.**, **Long, J.A.** ***et al.*** (2008) Rapid synthesis of auxin via a new tryptophan-dependent pathway is required for shade avoidance in plants. *Cell*, **133**(1), 164–176.

Umer, M.J., **Lu, Q.**, **Huang, L.**, **Batool, R.**, **Liu, H.**, **Li, H.** ***et al.*** (2024) Genome-wide association study reveals the genetic basis of amino acids contents variations in Peanut (*Arachis hypogaea* L.). *Physiologia Plantarum*, **176** (5), e14542.

Wang, C., **Ma, Q.**, **Xie, X.**, **Zhang, X.**, **Yang, D.**, **Su, J.** ***et al.*** (2022) Identification of favorable haplotypes/alleles and candidate genes for three plant architecture-related traits via a restricted two-stage multilocus genome-wide association study in upland cotton. *Industrial Crops and Products*, **177**, 114458.

Wang, M.L., **Wang, H.**, **Zhao, C.**, **Tonnis, B.**, **Tallury, S.**, **Wang, X.** ***et al.*** (2022) Identification of QTLs for seed dormancy in cultivated peanut using a recombinant inbred line mapping population. *Plant Molecular Biology Reporter*, **40**(1), 208–217.

Wang, Z., **Huai, D.**, **Zhang, Z.**, **Cheng, K.**, **Kang, Y.**, **Wan, L.** ***et al.*** (2018) Development of a high-density genetic map based on specific length amplified fragment sequencing and its application in quantitative trait loci analysis for yield-related traits in cultivated peanut. *Frontiers in Plant Science*, **9**, 827.

Wu, Y., **Sun, Z.**, **Qi, F.**, **Tian, M.**, **Wang, J.**, **Zhao, R.** ***et al.*** (2022) Comparative transcriptomics analysis of developing peanut (*Arachis hypogaea* L.) pods reveals candidate genes affecting peanut seed size. *Frontiers in Plant Science*, **13**, 958808.

Xavier, A., **Jarquin, D.**, **Howard, R.**, **Ramasubramanian, V.**, **Specht, J.E.**, **Graef, G.L.** ***et al.*** (2018) Genome-wide analysis of grain yield stability and environmental interactions in a multiparental soybean population. *G3: Genes, Genomes, Genetics*, **8**(2), 519–529.

Yamamoto, Y., **Kamiya, N.**, **Morinaka, Y.**, **Matsuoka, M.** & **Sazuka, T.** (2007) Auxin biosynthesis by the YUCCA genes in rice. *Plant Physiology*, **143**(3), 1362–1371.

Yan, J., **Warburton, M.** & **Crouch, J.** (2011) Association mapping for enhancing maize (*Zea mays* L.) genetic improvement. *Crop Science*, **51**(2), 433–449.

Yang, F., **Gu, Q.**, **He, W.**, **Hong, D.**, **Yu, M.** & **Yao, J.** (2025) Genetic basis of agronomic traits in cucumber: a review of QTL mapping studies. *Molecular Plant Breeding*, **16**, 1–12.

Yang, J., **Yue, Y.**, **Chen, C.**, **Chen, W.**, **Chen, Y.** & **Zhang, H.** (2025) Unraveling the genetic architecture of peanut pod-related traits via genome-wide association study. *Plant Molecular Biology Reporter*, **43**, 1–1306.

Ye, X., **Sun, J.**, **Tian, Y.**, **Chen, J.**, **Yao, X.**, **Quan, X.** ***et al.*** (2024) Identification of YUC genes associated with leaf wrinkling trait in Tacai variety of Chinese cabbage. *PeerJ*, **12**, e17337.

Yin, D., **Ji, C.**, **Ma, X.**, **Li, H.**, **Zhang, W.**, **Li, S.** ***et al.*** (2018) Genome of an allotetraploid wild peanut *Arachis monticola*: a de novo assembly. *GigaScience*, **7**(6), giy066.

Zhang, S., **Hu, X.**, **Miao, H.**, **Chu, Y.**, **Cui, F.**, **Yang, W.** ***et al.*** (2019) QTL identification for seed weight and size based on a high-density SLAF-seq genetic map in peanut (*Arachis hypogaea* L.). *BMC Plant Biology*, **19**, 1–15.

Zhang, X., **Zhu, L.**, **Ren, M.**, **Xiang, C.**, **Tang, X.**, **Xia, Y.** ***et al.*** (2023) Genome-wide association studies revealed the genetic loci and candidate genes of pod-related traits in peanut (*Arachis hypogaea* L.). *Agronomy*, **13**(7), 1863.

Zhao, C., **Qiu, J.**, **Agarwal, G.**, **Wang, J.**, **Ren, X.**, **Xia, H.** ***et al.*** (2017) Genome-wide discovery of microsatellite markers from diploid progenitor species, *Arachis duranensis* and *A. ipaensis*, and their application in cultivated peanut (*A. hypogaea*). *Frontiers in Plant Science*, **8**, 1209.

Zhao, Y. (2012) Auxin biosynthesis: a simple two-step pathway converts tryptophan to indole-3-acetic acid in plants. *Molecular Plant*, **5**(2), 334–338.

Zhao, Y., **Christensen, S.K.**, **Fankhauser, C.**, **Cashman, J.R.**, **Cohen, J.D.**, **Weigel, D.** ***et al.*** (2001) A role for flavin monooxygenase-like enzymes in auxin biosynthesis. *Science*, **291**(5502), 306–309.

Zheng, Z., **Sun, Z.**, **Qi, F.**, **Fang, Y.**, **Lin, K.**, **Pavan, S.** ***et al.*** (2024) Chloroplast and whole-genome sequencing shed light on the evolutionary history and phenotypic diversification of peanuts. *Nature Genetics*, **56**, 1–1984.

Zhou, X., **Guo, J.**, **Pandey, M.K.**, **Varshney, R.K.**, **Huang, L.**, **Luo, H.** ***et al.*** (2021) Dissection of the genetic basis of yield-related traits in the Chinese peanut mini-core collection through genome-wide association studies. *Frontiers in Plant Science*, **12**, 637284.

Zhuang, W., **Chen, H.**, **Yang, M.**, **Wang, J.**, **Pandey, M.K.**, **Zhang, C.** ***et al.*** (2019) The genome of cultivated peanut provides insight into legume karyotypes, polyploid evolution and crop domestication. *Nature Genetics*, **51**(5), 865–876.